LP2005-161
EPS2005-499

Improved Measurements of Branching Fractions and CP Asymmetries for $B \to \omega h$ Decays.

K. Abe,[9] K. Abe,[47] I. Adachi,[9] H. Aihara,[49] K. Aoki,[23] K. Arinstein,[2] Y. Asano,[54] T. Aso,[53] V. Aulchenko,[2] T. Aushev,[13] T. Aziz,[45] S. Bahinipati,[5] A. M. Bakich,[44] V. Balagura,[13] Y. Ban,[36] S. Banerjee,[45] E. Barberio,[22] M. Barbero,[8] A. Bay,[19] I. Bedny,[2] U. Bitenc,[14] I. Bizjak,[14] S. Blyth,[25] A. Bondar,[2] A. Bozek,[29] M. Bračko,[9,21,14] J. Brodzicka,[29] T. E. Browder,[8] M.-C. Chang,[48] P. Chang,[28] Y. Chao,[28] A. Chen,[25] K.-F. Chen,[28] W. T. Chen,[25] B. G. Cheon,[4] C.-C. Chiang,[28] R. Chistov,[13] S.-K. Choi,[7] Y. Choi,[43] Y. K. Choi,[43] A. Chuvikov,[37] S. Cole,[44] J. Dalseno,[22] M. Danilov,[13] M. Dash,[56] L. Y. Dong,[11] R. Dowd,[22] J. Dragic,[9] A. Drutskoy,[5] S. Eidelman,[2] Y. Enari,[23] D. Epifanov,[2] F. Fang,[8] S. Fratina,[14] H. Fujii,[9] N. Gabyshev,[2] A. Garmash,[37] T. Gershon,[9] A. Go,[25] G. Gokhroo,[45] P. Goldenzweig,[5] B. Golob,[20,14] A. Gorišek,[14] M. Grosse Perdekamp,[38] H. Guler,[8] R. Guo,[26] J. Haba,[9] K. Hara,[9] T. Hara,[34] Y. Hasegawa,[42] N. C. Hastings,[49] K. Hasuko,[38] K. Hayasaka,[23] H. Hayashii,[24] M. Hazumi,[9] T. Higuchi,[9] L. Hinz,[19] T. Hojo,[34] T. Hokuue,[23] Y. Hoshi,[47] K. Hoshina,[52] S. Hou,[25] W.-S. Hou,[28] Y. B. Hsiung,[28] Y. Igarashi,[9] T. Iijima,[23] K. Ikado,[23] A. Imoto,[24] K. Inami,[23] A. Ishikawa,[9] H. Ishino,[50] K. Itoh,[49] R. Itoh,[9] M. Iwasaki,[49] Y. Iwasaki,[9] C. Jacoby,[19] C.-M. Jen,[28] R. Kagan,[13] H. Kakuno,[49] J. H. Kang,[57] J. S. Kang,[16] P. Kapusta,[29] S. U. Kataoka,[24] N. Katayama,[9] H. Kawai,[3] N. Kawamura,[1] T. Kawasaki,[31] S. Kazi,[5] N. Kent,[8] H. R. Khan,[50] A. Kibayashi,[50] H. Kichimi,[9] H. J. Kim,[18] H. O. Kim,[43] J. H. Kim,[43] S. K. Kim,[41] S. M. Kim,[43] T. H. Kim,[57] K. Kinoshita,[5] N. Kishimoto,[23] S. Korpar,[21,14] Y. Kozakai,[23] P. Križan,[20,14] P. Krokovny,[9] T. Kubota,[23] R. Kulasiri,[5] C. C. Kuo,[25] H. Kurashiro,[50] E. Kurihara,[3] A. Kusaka,[49] A. Kuzmin,[2] Y.-J. Kwon,[57] J. S. Lange,[6] G. Leder,[12] S. E. Lee,[41] Y.-J. Lee,[28] T. Lesiak,[29] J. Li,[40] A. Limosani,[9] S.-W. Lin,[28] D. Liventsev,[13] J. MacNaughton,[12] G. Majumder,[45] F. Mandl,[12] D. Marlow,[37] H. Matsumoto,[31] T. Matsumoto,[51] A. Matyja,[29] Y. Mikami,[48] W. Mitaroff,[12] K. Miyabayashi,[24] H. Miyake,[34] H. Miyata,[31] Y. Miyazaki,[23] R. Mizuk,[13] D. Mohapatra,[56] G. R. Moloney,[22] T. Mori,[50] A. Murakami,[39] T. Nagamine,[48] Y. Nagasaka,[10] T. Nakagawa,[51] I. Nakamura,[9] E. Nakano,[33] M. Nakao,[9] H. Nakazawa,[9] Z. Natkaniec,[29] K. Neichi,[47] S. Nishida,[9] O. Nitoh,[52] S. Noguchi,[24] T. Nozaki,[9] A. Ogawa,[38] S. Ogawa,[46] T. Ohshima,[23] T. Okabe,[23] S. Okuno,[15] S. L. Olsen,[8] Y. Onuki,[31] W. Ostrowicz,[29] H. Ozaki,[9] P. Pakhlov,[13] H. Palka,[29] C. W. Park,[43] H. Park,[18] K. S. Park,[43] N. Parslow,[44] L. S. Peak,[44] M. Pernicka,[12] R. Pestotnik,[14] M. Peters,[8] L. E. Piilonen,[56] A. Poluektov,[2] F. J. Ronga,[9] N. Root,[2]

M. Rozanska,[29] H. Sahoo,[8] M. Saigo,[48] S. Saitoh,[9] Y. Sakai,[9] H. Sakamoto,[17] H. Sakaue,[33] T. R. Sarangi,[9] M. Satapathy,[55] N. Sato,[23] N. Satoyama,[42] T. Schietinger,[19] O. Schneider,[19] P. Schönmeier,[48] J. Schümann,[28] C. Schwanda,[12] A. J. Schwartz,[5] T. Seki,[51] K. Senyo,[23] R. Seuster,[8] M. E. Sevior,[22] T. Shibata,[31] H. Shibuya,[46] J.-G. Shiu,[28] B. Shwartz,[2] V. Sidorov,[2] J. B. Singh,[35] A. Somov,[5] N. Soni,[35] R. Stamen,[9] S. Stanič,[32] M. Starič,[14] A. Sugiyama,[39] K. Sumisawa,[9] T. Sumiyoshi,[51] S. Suzuki,[39] S. Y. Suzuki,[9] O. Tajima,[9] N. Takada,[42] F. Takasaki,[9] K. Tamai,[9] N. Tamura,[31] K. Tanabe,[49] M. Tanaka,[9] G. N. Taylor,[22] Y. Teramoto,[33] X. C. Tian,[36] K. Trabelsi,[8] Y. F. Tse,[22] T. Tsuboyama,[9] T. Tsukamoto,[9] K. Uchida,[8] Y. Uchida,[9] S. Uehara,[9] T. Uglov,[13] K. Ueno,[28] Y. Unno,[9] S. Uno,[9] P. Urquijo,[22] Y. Ushiroda,[9] G. Varner,[8] K. E. Varvell,[44] S. Villa,[19] C. C. Wang,[28] C. H. Wang,[27] M.-Z. Wang,[28] M. Watanabe,[31] Y. Watanabe,[50] L. Widhalm,[12] C.-H. Wu,[28] Q. L. Xie,[11] B. D. Yabsley,[56] A. Yamaguchi,[48] H. Yamamoto,[48] S. Yamamoto,[51] Y. Yamashita,[30] M. Yamauchi,[9] Heyoung Yang,[41] J. Ying,[36] S. Yoshino,[23] Y. Yuan,[11] Y. Yusa,[48] H. Yuta,[1] S. L. Zang,[11] C. C. Zhang,[11] J. Zhang,[9] L. M. Zhang,[40] Z. P. Zhang,[40] V. Zhilich,[2] T. Ziegler,[37] and D. Zürcher[19]

(The Belle Collaboration)

[1]*Aomori University, Aomori*
[2]*Budker Institute of Nuclear Physics, Novosibirsk*
[3]*Chiba University, Chiba*
[4]*Chonnam National University, Kwangju*
[5]*University of Cincinnati, Cincinnati, Ohio 45221*
[6]*University of Frankfurt, Frankfurt*
[7]*Gyeongsang National University, Chinju*
[8]*University of Hawaii, Honolulu, Hawaii 96822*
[9]*High Energy Accelerator Research Organization (KEK), Tsukuba*
[10]*Hiroshima Institute of Technology, Hiroshima*
[11]*Institute of High Energy Physics, Chinese Academy of Sciences, Beijing*
[12]*Institute of High Energy Physics, Vienna*
[13]*Institute for Theoretical and Experimental Physics, Moscow*
[14]*J. Stefan Institute, Ljubljana*
[15]*Kanagawa University, Yokohama*
[16]*Korea University, Seoul*
[17]*Kyoto University, Kyoto*
[18]*Kyungpook National University, Taegu*
[19]*Swiss Federal Institute of Technology of Lausanne, EPFL, Lausanne*
[20]*University of Ljubljana, Ljubljana*
[21]*University of Maribor, Maribor*
[22]*University of Melbourne, Victoria*
[23]*Nagoya University, Nagoya*
[24]*Nara Women's University, Nara*
[25]*National Central University, Chung-li*
[26]*National Kaohsiung Normal University, Kaohsiung*
[27]*National United University, Miao Li*
[28]*Department of Physics, National Taiwan University, Taipei*

[29]H. Niewodniczanski Institute of Nuclear Physics, Krakow
[30]Nippon Dental University, Niigata
[31]Niigata University, Niigata
[32]Nova Gorica Polytechnic, Nova Gorica
[33]Osaka City University, Osaka
[34]Osaka University, Osaka
[35]Panjab University, Chandigarh
[36]Peking University, Beijing
[37]Princeton University, Princeton, New Jersey 08544
[38]RIKEN BNL Research Center, Upton, New York 11973
[39]Saga University, Saga
[40]University of Science and Technology of China, Hefei
[41]Seoul National University, Seoul
[42]Shinshu University, Nagano
[43]Sungkyunkwan University, Suwon
[44]University of Sydney, Sydney NSW
[45]Tata Institute of Fundamental Research, Bombay
[46]Toho University, Funabashi
[47]Tohoku Gakuin University, Tagajo
[48]Tohoku University, Sendai
[49]Department of Physics, University of Tokyo, Tokyo
[50]Tokyo Institute of Technology, Tokyo
[51]Tokyo Metropolitan University, Tokyo
[52]Tokyo University of Agriculture and Technology, Tokyo
[53]Toyama National College of Maritime Technology, Toyama
[54]University of Tsukuba, Tsukuba
[55]Utkal University, Bhubaneswer
[56]Virginia Polytechnic Institute and State University, Blacksburg, Virginia 24061
[57]Yonsei University, Seoul

(Dated: February 7, 2008)

Abstract

We report improved measurements of B to pseudoscalar-vector decays containing an ω meson in the final state. These results are obtained from a data sample that contains 386 million $B\bar{B}$ pairs collected at the $\Upsilon(4S)$ resonance, with the Belle detector at the KEKB asymmetric energy e^+e^- collider. We measure the branching fractions $\mathcal{B}(B^\pm \to \omega K^\pm) = (8.1 \pm 0.6 \pm 0.5) \times 10^{-6}$, $\mathcal{B}(B^\pm \to \omega \pi^\pm) = (7.0 \pm 0.6 \pm 0.5) \times 10^{-6}$, and $\mathcal{B}(B^0 \to \omega K^0) = (3.9 \pm 0.7 \pm 0.4) \times 10^{-6}$. We also set the 90% confidence level upper limit $\mathcal{B}(B^0 \to \omega \pi^0) < 1.5 \times 10^{-6}$. In addition, we obtain the partial rate asymmetries $\mathcal{A}_{CP} = 0.05 \pm 0.08 \pm 0.01$ for $B^\pm \to \omega K^\pm$ and $\mathcal{A}_{CP} = -0.03 \pm 0.09 \pm 0.02$ for $B^\pm \to \omega \pi^\pm$.

PACS numbers: PACS numbers: 13.20.H

Charmless hadronic B decays provide a rich ground to understand the dynamics of B meson decays and the origin of CP violation. Two-body B decays with a vector meson ω and a pseudoscalar particle h (h can be kaon or pion) proceed through $b \to s$ penguin diagrams and $b \to u$ diagrams. Theoretical expectations from QCD factorization approaches suggest that the branching fractions of charged B decays are be-

tween 3 and 8 $\times 10^{-6}$ and that the ωK^+ branching fraction is smaller than the $\omega\pi^+$ [1, 2]. The decay $B^0 \to \omega\pi^0$ is color suppressed while the neutral B decay to ωK^0 is expected to have slightly smaller branching fraction than the charged B decays. Experimentally, clear signals have been observed in $B^\pm \to \omega K^\pm, B^\pm \to \omega\pi^\pm$ and $B^0 \to \omega K^0$ with similar branching fractions [3, 4, 5]. However, experimental measurements are not yet precise enough to tell which mode has the larger branching fraction. Furthermore, the branching fraction of $B^0 \to \omega K^0$ measured by the Belle collaboration is smaller than the BaBar result. Therefore, it is necessary to update the results with more data.

In this paper, we report improved measurements of branching fractions and partial rate asymmetries for $B \to \omega h$ decays, where h can be a kaon or pion. The partial rate asymmetry ($\mathcal{A}_{CP}$) is measured for the charged B decays and defined to be

$$\mathcal{A}_{CP} \equiv \frac{\Gamma(B^- \to f^-) - \Gamma(B^+ \to f^+)}{\Gamma(B^- \to f^-) + \Gamma(B^+ \to f^+)}, \quad (1)$$

where $\Gamma(B^- \to f^-)$ is the B^- decay rate and $\Gamma(B^+ \to f^+)$ denotes that of the charge conjugate mode. These measurements are based on a data sample of 386 million $B\bar{B}$ pairs, collected with the Belle detector at the KEKB [6] asymmetric-energy e^+e^- collider. The statistics are a factor of 5 larger than our previous published results.

The Belle detector is a large-solid-angle magnetic spectrometer that consists of a silicon vertex detector (SVD), a 50-layer central drift chamber (CDC), an array of aerogel threshold Čerenkov counters (ACC), a barrel-like arrangement of time-of-flight scintillation counters (TOF), and an electromagnetic calorimeter comprised of CsI(Tl) crystals (ECL) located inside a super-conducting solenoid coil that provides a 1.5 T magnetic field. An iron flux-return located outside of the coil is instrumented to detect K_L^0 mesons and to identify muons (KLM). The detector is described in detail elsewhere [7]. In August 2003, the three-layer SVD was replaced by a four-layer radiation tolerant device. The data sample for this analysis consists of 140 fb^{-1} of data with the old SVD (Set I) and 217 fb^{-1} with the new one (Set II).

Hadronic events are selected using criteria based on the charged track multiplicity and total visible energy with an efficiency greater than 99% for generic $B\bar{B}$ events. All primary charged tracks must satisfy quality requirements based on their impact parameters relative to the run-dependent interaction point (IP). For tracks from the candidate B mesons, their deviations from the IP position are required to be within ± 0.1 cm in the transverse direction and ± 3.0cm in the longitudinal direction. Charged particle identification is performed using the K-π likelihood ratio, $\mathcal{R}_K = \mathcal{L}_K/(\mathcal{L}_\pi + \mathcal{L}_K)$, where $\mathcal{L}_K$ ($\mathcal{L}_\pi$) is the likelihood of a charged particle to be a kaon (pion) based on the information coming from ACC, TOF and CDC. Charged tracks from B meson candidates with $\mathcal{R}_K > 0.6$ are identified as kaons and $\mathcal{R}_K < 0.4$ as pions. Kaons produced in the $B^\pm \to \omega K^\pm$ decays are selected by these criteria with efficiencies 85%, while the corresponding rates of Kaons that are misidentified as pions are 11%; on the other hand, pions from $B^\pm \to \omega\pi^\pm$ are selected with an efficiency of 90% and a kaon misidentification rate of 9%. Candidate π^0 mesons are reconstructed from pairs of photons with invariant mass in the range $0.1178\ \mathrm{GeV/c^2} < M_{\gamma\gamma} < 0.1502\ \mathrm{GeV/c^2}$. Candidate K_S^0 mesons are reconstructed using pairs of oppositely charged particles that have an invariant mass in the range $0.482\ \mathrm{GeV/c^2} < M_{\pi^+\pi^-} < 0.514\ \mathrm{GeV/c^2}$. The vertex of the K_S^0 candidate is required to be well reconstructed and displaced from the interaction point, and the K_S^0 momentum direction must be consistent with the K_S^0 flight direction. Candidate $\omega \to \pi^+\pi^-\pi^0$ decays are reconstructed from charged tracks with $\mathcal{R}_K < 0.9$, where the pions from the ω decay are selected with 96% efficiency, and the π^0s with center-of-mass frame momentum are greater

than 0.35 GeV/c^2. Candidate ω mesons are required to have invariant masses within ± 30 MeV/c^2 of the nominal value.

B meson candidates are formed by combining an ω meson with either a kaon ($K^\pm$, K^0_S) or a pion ($\pi^\pm$, π^0). Two kinematic variables are used to select B candidates: the beam constrained mass $M_{\rm bc} = \sqrt{(E^{\rm CM}_{\rm beam})^2 - |P^{\rm CM}_B|^2}$ and the energy difference $\Delta E = E^{\rm CM}_B - E^{\rm CM}_{\rm beam}$, where $E^{\rm CM}_{\rm beam}$ is the beam energy in the $\Upsilon(4S)$ rest frame, and $P^{\rm CM}_B$, $E^{\rm CM}_B$ are the momentum and energy of the B candidate in the $\Upsilon(4S)$ rest frame. Candidates with $M_{\rm bc} > 5.2$ GeV/c^2 and $|\Delta E| < 0.25$ GeV ($|\Delta E| < 0.30$ GeV for $B^0 \to \omega\pi^0$) are selected for further analysis.

The dominant background comes from quark-antiquark continuum events ($e^+e^- \to q\bar{q}$, $q = u,d,s,c$). The continuum background is characterized by a jet-like structure while the $B\bar{B}$ events have a more spherical distribution. Several event-shape variables are employed to suppress the continuum. The thrust angle θ_T is defined as the angle between the thrust axis [8] of the B candidate daughter particles and that of the rest of the particles in an event. Signal events are uniformly distributed in $\cos\theta_T$, while continuum events are sharply peaked near $\cos\theta_T = \pm 1.0$. Events with $|\cos\theta_T| < 0.9$ are selected. A Fisher discriminant is formed by combining a set of modified Fox-Wolfram moments [9] with the variable $S_\perp$, defined as the scalar sum of the transverse momentum of all particles outside a 45° cone around the thrust axis of the B candidate divided by the scalar sum of their momenta. Further variables that have been found to separate signal from continuum background include: the cosine of the angle between the flight direction of the B candidate and the beam direction ($\cos\theta_B$), the distance along the beam direction between the B vertex and the vertex of the remaining particles of the event (Δz) and the cosine of the helicity angle, defined as the angle between the B flight direction in the ω rest frame and the normal direction of the plane spanned by the three daughter pions of the ω. The probability density functions (PDFs) for these three variables and the Fisher discriminant are obtained using events in signal Monte Carlo simulation and data with $M_{\rm bc} < 5.26$ GeV/c^2 for signal and $q\bar{q}$ background, respectively. These variables are combined to form a likelihood ratio $\mathcal{R} = \frac{\mathcal{L}_S}{\mathcal{L}_S + \mathcal{L}_{q\bar{q}}}$, where $\mathcal{L}_{S(q\bar{q})}$ is the product of signal ($q\bar{q}$) probability densities.

Additional background discrimination is provided by the quality of the B flavor tagging of the accompanying B meson. We use the standard Belle B tagging package [10], which gives two outputs: a discrete variable (q) indicating the B flavor and a dilution factor (r) ranging from zero for no flavor information to unity for unambiguous flavor assignment. We divide the data into six r regions. Continuum suppression is achieved by applying a mode dependent requirement on $\mathcal{R}$ for events in each r region based on $\mathcal{N}_s/\sqrt{\mathcal{N}_s + \mathcal{N}_{q\bar{q}}}$, where $\mathcal{N}_s$ is the expected number of signal events estimated from simulation and $\mathcal{N}_{q\bar{q}}$ denotes the number of background events estimated from data. This $\mathcal{R}$ requirement retains 74%, 68%, 74%, and 57% of the signal while rejecting 91%, 94%, 91%, and 95% of the continuum background for the $\omega K^\pm$, $\omega\pi^\pm$, ωK^0, and $\omega\pi^0$ modes, respectively.

Simulation studies indicate small backgrounds from generic $b \to c$ transitions in the charged B modes; they are found to be negligible for the neutral modes. Moreover, two other backgrounds need to be considered: the $\omega K^+ \leftrightarrow \omega\pi^+$ reflection, due to $K^+ \leftrightarrow \pi^+$ misidentification, and the feed-down from charmless B decays, predominantly $B \to \omega K^*(892)$ and $B \to \omega\rho(770)$. We include these three components in the fit used to extract the signal.

The signal yields and partial rate asymmetries are obtained using an extended unbinned maximum likelihood fit on $M_{\rm bc}$ and

ΔE. The likelihood is defined as

$$\mathcal{L} = e^{-\sum_j \mathcal{N}_j} \times \prod_i (\sum_j \mathcal{N}_j \mathcal{P}_j) \quad (2)$$

$$\mathcal{P}_j = \frac{1}{2}[1 - Q_i \cdot \mathcal{A}_{CPj}] P_j(M_{bci}, \Delta E_i) \quad (3)$$

where i is the identifier of the i-th event, $P(M_{bc}, \Delta E)$ is the PDF of M_{bc} and ΔE, Q indicates the B meson charge, $B^+(Q = +1)$ or $B^-(Q = -1)$, $\mathcal{N}_j$ is the number of events for the category j, which corresponds to either signal, $q\bar{q}$ continuum, a reflection due to K-π misidentification, or $B\bar{B}$ backgrounds, inclusive of $b \to c$ background and other charmless B decays. For the neutral B mode, $\mathcal{P}_j$ in Eq.(2) is simply $P_j(M_{bci}, \Delta E_i)$ and there is no reflection component and $b \to c$ background.

The signal distribution in M_{bc} is parameterized by a Gaussian function centered near the mass of the B meson, while the Crystal-Ball line shape [11] is used to model the ΔE distribution. The product of the two functions is used as the signal PDF, calibrated with large control samples of $B \to D\pi, \overline{D}^0 \to K^+\pi^-\pi^0$ and $B \to \eta'(\eta\pi^+\pi^-)K$ decays. The continuum PDF is the product of a first order polynomial for ΔE and an ARGUS function [12] for M_{bc}. Other background PDFs are modelled by a smoothed two-dimensional $M_{bc} - \Delta E$ function obtained from the MC simulation. The yields of the $B\bar{B}$ background mentioned in the previous paragraph are fixed with $\mathcal{A}_{CP} = 0$ in the fit based on the MC simulation except for the reflection component. The $\mathcal{A}_{CP}$ and the normalizations of the reflection components are fixed to expectations based on the $B^+ \to \omega K^+$ and $B^+ \to \omega\pi^+$ partial rate asymmetries and branching fractions, as well as $K^+ \leftrightarrow \pi^+$ fake rates. The reflection yield and $\mathcal{A}_{CP}$ are first input with the assumed values and are then recalculated according to our measured results.

Table I and Table II show the measured branching fractions and $\mathcal{A}_{CP}$ as well as other quantities associated with the measurements. Branching fractions are computed as the sum of the yields divided by the corresponding efficiencies in each dataset, divided by the total number of B mesons. The reconstruction efficiency for each mode is defined as the fraction of the signal yield remaining after all selection criteria, where the yield is determined by performing the unbinned maximum likelihood fit on the MC sample. We define the significance as $\sqrt{-2\ln(\mathcal{L}_0/\mathcal{L}_{max})}$, where $\mathcal{L}_{max}$ is the maximum likelihood from the fit when the signal branching fraction is floated, and $\mathcal{L}_0$ is the likelihood obtained when the signal branching fraction is set to zero. Systematic uncertainties are included by repeating the fit with all parameters fixed at $\pm 1\sigma$ from their central value and choosing the set of parameters that gives the smallest significance.

For the branching fraction measurement, the main sources of systematic uncertainties are: charged tracking efficiency (1.0% per track); neutral pion detection (3.5% for Set I and 4.0% for Set II); K^0_S reconstruction (4.5% for Set I and 4.0% for Set II); ω mass resolution (0.2% for Set I and 0.6% for Set II); requirement on $\mathcal{R}$ (about 3.0%). Systematic uncertainties due to fit parameters are evaluated by varying each of the fixed parameters by $\pm 1\sigma$, and by adding in quadrature the resulting deviations from the central value. The total systematic uncertainty is the quadratic sum of all the above contributions.

In summary, we update the measurements of the branching fractions of the exclusive two-body charmless hadronic B decays with an ω meson in the final state. We measure the following branching fractions: $\mathcal{B}(B^\pm \to \omega K^\pm) = (8.1 \pm 0.6 \pm 0.5) \times 10^{-6}$, $\mathcal{B}(B^\pm \to \omega\pi^\pm) = (7.0 \pm 0.6 \pm 0.5) \times 10^{-6}$, and $\mathcal{B}(B^0 \to \omega K^0) = (3.9 \pm 0.7 \pm 0.4) \times 10^{-6}$. We also set the following upper limit: $\mathcal{B}(B^0 \to \omega\pi^0) < 1.5 \times 10^{-6}$ at the 90% confidence level. Finally, we measure the partial rate asymmetries in $B^\pm \to \omega K^\pm$ and $B^\pm \to \omega\pi^\pm$: $\mathcal{A}_{CP} = 0.05 \pm 0.08 \pm 0.01$ for $\omega K^\pm$, and $\mathcal{A}_{CP} = -0.03 \pm 0.09 \pm 0.02$ for $\omega\pi^\pm$; no evidences of direct CP violation is found in ei-

TABLE I: Signal yields ($\mathcal{N}_s$), efficiencies (ϵ_{tot}), fitted branching fraction ($\mathcal{B}$), partial rate asymmetry ($\mathcal{A}_{CP}$), and fit significance including systematic error (Σ) for the $B^\pm \to \omega K^\pm$ and $B^\pm \to \omega\pi^\pm$ modes.

Mode	$\omega K^\pm$	$\omega\pi^\pm$
$\mathcal{N}_s$ (SetI)	90^{+12}_{-11}	84^{+12}_{-11}
$\mathcal{N}_s$ (SetII)	170 ± 16	145 ± 16
ϵ_{tot} (SetI)	8.6 ± 0.1 %	9.1 ± 0.1 %
ϵ_{tot} (SetII)	8.5 ± 0.1 %	8.6 ± 0.1 %
$\mathcal{B}$ ($\times 10^{-6}$)	$8.1 \pm 0.6 \pm 0.5$	$7.0 \pm 0.6 \pm 0.5$
$\mathcal{A}_{CP}$	$0.05 \pm 0.08 \pm 0.01$	$-0.03 \pm 0.09 \pm 0.02$
Σ	20.0σ	17.3σ

TABLE II: Signal yields ($\mathcal{N}_s$), efficiencies (ϵ_{tot}), fitted branching fraction ($\mathcal{B}$), upper limit on the branching fraction (U.L.) including systematic error, and fit significance including systematic error (Σ) for the $B^0 \to \omega K^0$ and $B^0 \to \omega\pi^0$ modes.

Mode	ωK^0	$\omega\pi^0$
$\mathcal{N}_s$ (SetI)	$16^{+5.0}_{-4.4}$	–
$\mathcal{N}_s$ (SetII)	$14^{+5.1}_{-4.4}$	$2.8^{+4.7}_{-4.4}$
ϵ_{tot} (SetI)	2.7 ± 0.1 %	4.7 ± 0.1 %
ϵ_{tot} (SetII)	2.8 ± 0.1 %	3.7 ± 0.1 %
$\mathcal{B}$ ($\times 10^{-6}$)	$3.9 \pm 0.7 \pm 0.4$	$0.8^{+0.5}_{-0.4} \pm 0.1$
U.L. ($\times 10^{-6}$)	–	1.5
Σ	9.3σ	2.2σ

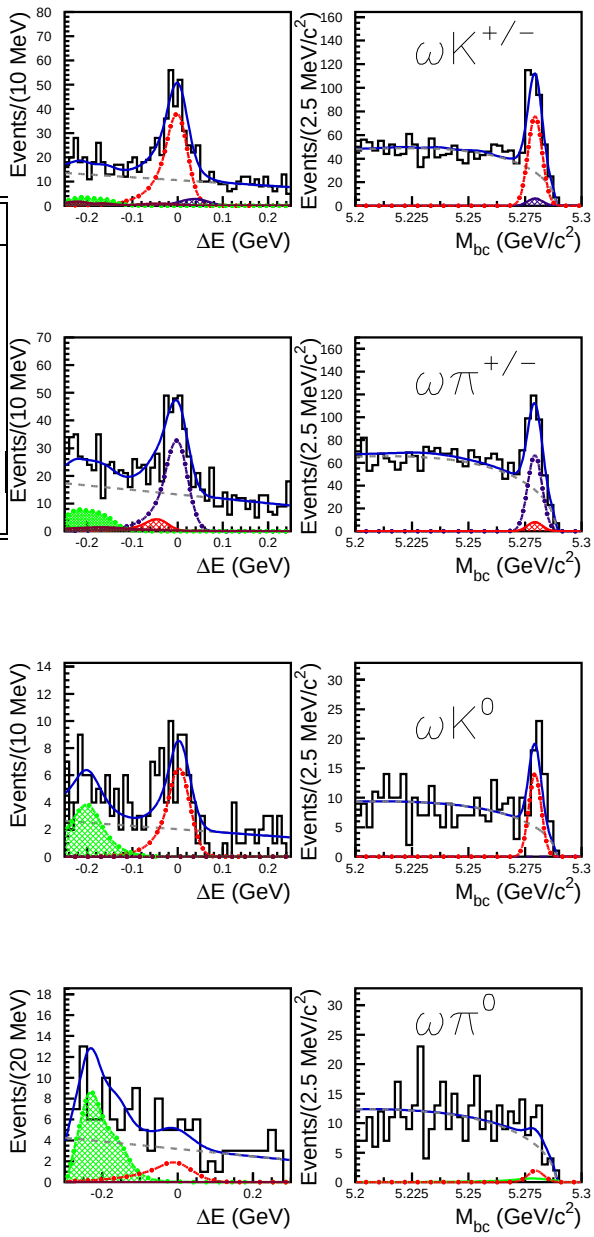

FIG. 1: Projections of fit results on $M_{\rm bc}$ (within the region of $|\Delta E| \leq 0.1$, $-0.15 \leq \Delta E \leq 0.1$ for $\omega\pi^0$) and ΔE (within the region of $5.27 < M_{\rm bc} < 5.29$) for $\omega K^\pm$, $\omega\pi^\pm$, ωK^0, and $\omega\pi^0$. Open histograms are data, solid curves are the fit functions, dash-dotted lines represent signals, the dashed lines show the $q\bar{q}$ continuum, light gray crossed-hatched areas represent rare B decay backgrounds, dark gray hatched areas peaking in the $M_{\rm bc}$ signal region represent reflections due to K-π misidentification and the small dark-gray contributions in the negative ΔE region of the charged modes are due to generic $B\bar{B}$ background.

ther mode so far.

We thank the KEKB group for the excellent operation of the accelerator, the KEK cryogenics group for the efficient operation of the solenoid, and the KEK computer group and the National Institute of Informatics for valuable computing and Super-SINET network support. We acknowledge support from the Ministry of Education, Culture, Sports, Science, and Technology of Japan and the Japan Society for the Promotion of Science;

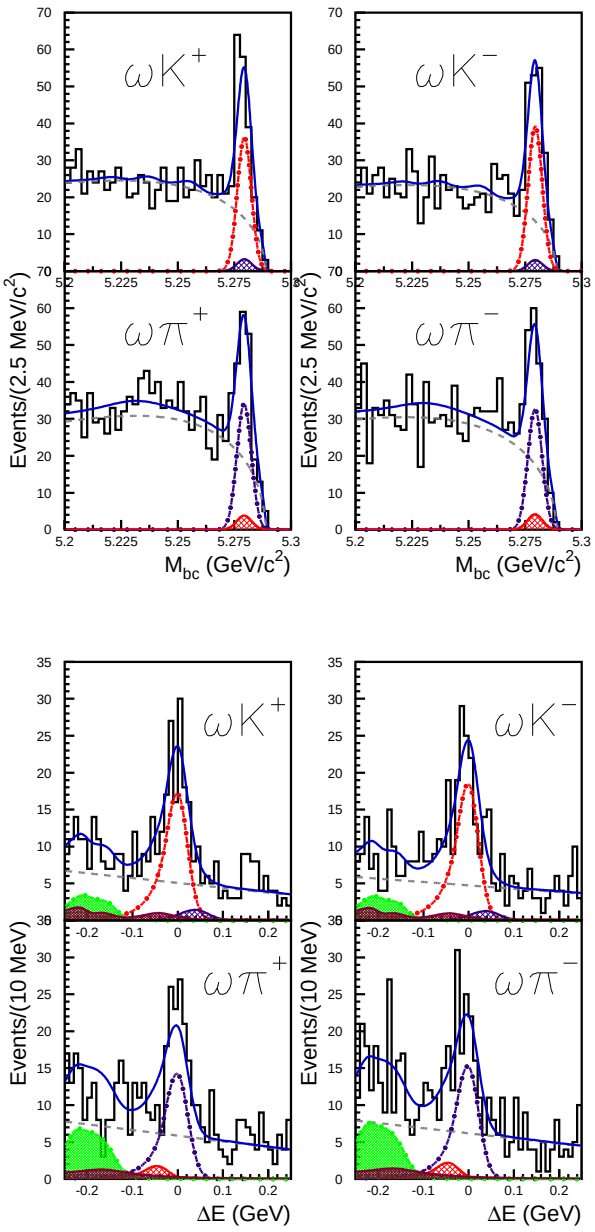

FIG. 2: Projections of fit results on $M_{\rm bc}$ (within the region of $|\Delta E| \leq 0.1$, $-0.15 \leq \Delta E \leq 0.1$ for $\omega\pi^0$) and ΔE (within the region of $5.27 < M_{\rm bc} < 5.29$) for $\omega K^{\pm}$, $\omega\pi^{\pm}$, ωK^0, and $\omega\pi^0$. Open histograms are data, solid curves are the fit functions, dash-dotted lines represent signals, the dashed lines show the $q\bar{q}$ continuum, light gray crossed-hatched areas represent rare B decay backgrounds, dark gray hatched areas peaking in the $M_{\rm bc}$ signal region represent reflections due to K-π misidentification and the small dark-gray contributions in the negative ΔE region are due to generic $B\bar{B}$ background.

the Australian Research Council and the Australian Department of Education, Science and Training; the National Science Foundation of China under contract No. 10175071; the Department of Science and Technology of India; the BK21 program of the Ministry of Education of Korea, and the CHEP SRC program and Basic Reserch program (grant No. R01-2005-000-10089-0) of the Korea Science and Engineering Foundation; the Polish State Committee for Scientific Research under contract No. 2P03B 01324; the Ministry of Science and Technology of the Russian Federation; the Ministry of Higher Education, Science and Technology of the Republic of Slovenia; the Swiss National Science Foundation; the National Science Council and the Ministry of Education of Taiwan; and the U.S. Department of Energy.

[1] M. Beneke and M. Neubert, Nucl. Phys. B **675**, 333 (2003).

[2] C.-H. Chen, Phys. Lett. B **525**, 56 (2002); Y.Y. Keum and A.I. Sanda, Phys. Rev.**D67**, 054009 (2003).

[3] Belle Collaboration, C.H. Wang *et al.*, Phys. Rev.**D70**, 012001 (2004).

[4] BaBar Collaboration, B. Aubert *et al.*, Phys. Rev.**D71**, 031103 (2005).

[5] BaBar Collaboration, B. Aubert *et al.*, hep-ex/0503018.

[6] S. Kurokawa and E. Kikutani, Nucl. Instr. and. Meth. A **499**, 1 (2003), and other papers included in this volume.

[7] Belle Collaboration, A. Abashian *et al.*, Nucl. Instr. and Meth. A **479**, 117 (2002).

[8] We define the thrust axis for a collection of particles as the axis that maximizes the sum of the magnitude of the longitudinal momenta with respect to the axis.

[9] The Fox-Wolfram moments were introduced in G. C. Fox and S. Wolfram, Phys. Rev. Lett. **41**, 1581 (1978). The Fisher discriminant used by Belle, based on modified

Fox-Wolfram moments (SFW), is described in K. Abe *et al.* (Belle Collab.), Phys. Rev. Lett. **87**, 101801 (2001) and K. Abe *et al.* (Belle Collab.), Phys. Lett. B **511**, 151 (2001).

[10] Belle Collaboration, H. Kakuno *et al.*, Nucl. Instr. and Meth.A **533**, 516 (2004).

[11] Crystal Ball Collaboration, J.E. Gaiser *et al.*, Phys. Rev. D **34**, 711 (1986).

[12] ARGUS Collaboration, H. Albrecht *et al.*, Phys. Lett. B **241**, 278 (1990).